Mon. Not. R. astr. Soc. (1983) **204,** 891–907

Three-dimensional numerical model of the formation of large-scale structure in the Universe

A. A. Klypin and S. F. Shandarin *The Keldysh Institute of Applied Mathematics, Academy of Sciences of USSR, Miusskaja Sq. 4, Moscow 125047, USSR*

Received 1982 November 15; in original form 1982 April 28

Summary. The first results of numerical fully three-dimensional simulations of formation and evolution of the large-scale structure of the Universe are presented. The simulations were carried out in the framework of the adiabatic scenario of galaxy formation.

The model contains $32^3 = 32\,768$ collisionless particles interacting only gravitationally. Equal mass particles are moving in a collective gravitational field which is smoothed at small scales. Evolution of perturbations is followed in an expanding cosmological model.

The numerical procedure starts at $z_{\text{start}} \simeq 5.25$, when $(\delta\rho/\rho)_{r_0} \simeq 0.22$ and $r_0 = 5\,h_{100}^{-1}$ Mpc is our cell length. Previous evolution was computed in accord with the approximate non-linear solution by Zeldovich. The initial perturbations of density as well as velocity were taken as a Fourier sum with random coefficients ranging from $\lambda_{\min} \simeq 40\,h_{100}^{-1}$ Mpc up to $\lambda_{\max} \simeq 160\,h_{100}^{-1}$ Mpc. The latter is the size of the cube where particles travel. The total number of cells to solve the Poisson equation is 32^3, thus the shortest wavelength in the initial perturbations contains eight cells.

The structure formation begins from pancakes, then evolves to the network structure, then to formation of clumps connected by strings and afterwards to formation of huge isolated clumps. Because of statistical initial perturbations one can observe different phases of the process in different places simultaneously.

The two-point correlation function was calculated. The model correlation function is shown to agree reasonably over the range $1 \gtrsim \xi \gtrsim 0.05$ with the observational one. We were mainly interested in the scale $5\,h_{100}^{-1}$ Mpc $\lesssim r \lesssim 160\,h_{100}^{-1}$ Mpc; the smaller as well as larger scales were beyond the opportunity of our simulations. The mass function of clumps agree reasonably with that of Abell clusters.

1 Introduction

Recent observations of the large-scale galaxy distribution urge theorists to develop more and more realistic models of the formation of structure in the Universe. Numerical simulation of self-gravitating systems is very important.

Three-dimensional numerical experiments have been carried out in the framework of the isothermal scenario of galaxy formation (for example, Fall 1978; Aarseth, Gott & Turner 1979; Gott, Turner & Aarseth 1979; Efstathiou & Jones 1979; Efstathiou 1979; Efstathiou & Eastwood 1981). In these works most attention was paid to the evolution of the correlation function and formation of groups and clusters. However, a very important feature of the large-scale structure, an existence of flattened objects similar to the Local Supercluster (de Vaucouleurs 1976; Tully 1982) and elongated ones similar to the Perseus chain (Einasto, Joever & Saar 1980), have not found an explanation in the isothermal picture.

The large voids of galaxies discovered in recent years (Gregory & Thompson 1978; Einasto *et al.* 1980; Kirshner *et al.* 1981) make another, probably more serious, challenge to the isothermal scenario (Zeldovich & Shandarin 1982). On the other hand, this structure is inevitable in the adiabatic picture (Zeldovich 1978 and references therein). However, until now there were no necessary estimates of the correlation function in this scenario.

Studying the evolution of adiabatic perturbations, Zeldovich (1970) showed that objects forming at the non-linear stage must have a very flattened shape. Due to their shape they were called 'pancakes'. Afterwards it was found that a pancake is a particular type of a few generic singularities arising in potential flows of a cold medium (Arnold 1972; Arnold Zeldovich & Shandarin 1982). Pancakes are a specific kind of singularities as they give birth to the large-scale structure. The subsequent evolution, as it was shown in the two-dimensional simulation (Doroshkevich *et al.* 1980) leads to intersection of the pancakes and to formation of the well-pronounced cellular structure.

In this paper we present the first results of three-dimensional numerical simulations of the large-scale structure formation in the adiabatic scenario. These results show that the theory explains two observational facts: (i) the power-law shape of the two-point spatial correlation function over the range $1 \gtrsim \xi \gtrsim 0.05$ (with the power index $\gamma \simeq 1.8$) and (ii) existence of prolate filaments connecting the clusters.

Our numerical experiments show that the filaments form later than the pancakes. However, they have much stronger concentration of density and therefore one can observe them much more easily. This is in qualitative agreement with the general theory of singularities (Arnold *et al.* 1982 and references therein) and the observations (Einasto *et al.* 1980).

In the present paper we pay more attention to the most interesting qualitative results. Many other questions will be discussed in detail in subsequent works. These results are useful first of all for the adiabatic scenario in the neutrino dominated Universe (Doroshkevich *et al.* 1981).

Our model is described briefly in Section 2 and the technique of simulation is considered in Section 3. Section 4 is devoted to a description of the model evolution. In Sections 5 and 6 we give estimations of the two-point correlation function and the mass function of rich clusters. Section 7 contains a short discussion of the main results.

2 Model

The Einstein–de Sitter universe ($\Omega = 1$) is considered. Initial perturbations are generated in a random process and have a flat spectrum of density contrast in the range of scales restricted both above and below. For the sake of convenience the computations were carried out in coordinates comoving with the mean expansion of the Universe (Shandarin 1980).

The main problem is to compute motion of a large number of particles in the gravitational field created by them. Since we are interested only in properties of the large-scale structure, the smoothed potential technique is the most suitable one. In accordance with this

technique, each particle is treated as moving in the collective field of all others, although the influence of its closest neighbours comes into account with some inaccuracy.

The total number of equal mass particles in the model is $32^3 = 32\,768$. We used the wide spread CIC ('cloud-in-cell') method. The fast Fourier transformation is applied when solving a system of 32 768 linear equations arising after discretization of the Poisson equation (Hockney 1970).

The region within which the particles were allowed to move is a cube with the side being equal to $32r_0$. Here $r_0 = 5h^{-1}$ Mpc is the linear size of a cell, $h = H_0/(100\,\mathrm{km\,s^{-1}\,Mpc^{-1}})$. Boundary conditions are periodic, thus a particle coming out of the cube returns back on the opposite side with the same velocity.

At initial time density perturbations on the scale r_0 were $(\delta\rho/\rho)_{r_0} \simeq 0.2$. After this the evolution of the system is treated numerically till the time when density perturbations reach the value of $(\delta\rho/\rho)_{r_0} \simeq 4.8$. For the whole time the expansion factor increases by a factor of 22.

In numerical simulations done in the framework of the isothermal scenario the generation of initial conditions is simple. Usually initial conditions were produced by choosing randomly the positions of the particles in some region of space. The velocities were fixed according to the Hubble law, sometimes with peculiar components (Aarseth *et al.* 1979). In the case of the adiabatic models this method cannot be applied because it is necessary to distribute the particles in such a way that the spectrum of density fluctuations should not contain short harmonics.

In this work we used the non-linear theory of gravitational instability (Zeldovich 1970) as a basis to produce the initial conditions. Only the growing mode of perturbations was involved. The application of the non-linear theory permits us to start the calculations from the moment when perturbations are rather large.

Let $\mathbf{q}$ be a fixed Lagrangian (unperturbed) coordinate of a particle at $z = 0$ and $\partial S/\partial \mathbf{q}$ be the relevant vector of the particle displacement from the homogeneous state. Then, according to the non-linear theory, the coordinates and velocities in a growing mode are (we assume $\Omega = \bar{\rho}/\rho_c = 1$)

$$r_i = a(t)\left[q_i - \left(\frac{t}{t_H}\right)^{2/3} \frac{\partial S}{\partial q_i}\right], \tag{1}$$

$$v_i = \frac{da}{a\,dt} r_i - \frac{2}{3t_H}\left(\frac{t}{t_H}\right)^{1/3} \frac{\partial S}{\partial q_i}, \qquad t_H = \frac{2}{3H_0}, \qquad a(t) = \left(\frac{t}{t_H}\right)^{2/3}, \tag{2}$$

where H_0 is the Hubble constant at $z = 0$ and $a(t)$ is the expansion factor. Function S is assumed to be a three-dimensional Fourier sum:

$$S(\mathbf{q}) = \alpha \sum_{k_1=-k_{\max}}^{k_{\max}} \sum_{k_2=-k_{\max}}^{k_{\max}} \sum_{k_3=-k_{\max}}^{k_{\max}} [A(\mathbf{k})\cos(\mathbf{kq}) + B(\mathbf{k})\sin(\mathbf{kq})]/k^2,$$
$$k_{1,2,3} = \pi l/16 r_0, \qquad l = 0, \pm 1, \ldots \pm 4, \qquad k^2 = k_1^2 + k_2^2 + k_3^2 \neq 0. \tag{3}$$

Here $A(\mathbf{k})$ and $B(\mathbf{k})$ are Gaussian random numbers with $\langle A \rangle = \langle B \rangle = 0$ and $\langle A^2 \rangle = \langle B^2 \rangle = 1$, α is the amplitude of perturbations. The value $k_{\max}$ is equal to $\pi/4r_0$ (that is, the shortest wavelengths in the initial density spectrum correspond to eight particles and eight cells).

One can easily find that in the linear approximation the density contrast of the matter is

$$\delta\rho/\rho = -\alpha \sum_{-k_{\max}}^{k_{\max}} \sum \sum [A(\mathbf{k})\cos(\mathbf{kq}) + B(\mathbf{k})\sin(\mathbf{kq})]. \tag{4}$$

So equations (1)–(3) determine an approximately flat spectrum of density fluctuations with rms Fourier components equal to α. We have chosen $\alpha = 8 \times 10^{-3}$ ($z = 5.25$).*

All calculations were carried out in dimensionless comoving coordinates. In order to return to real dimensional values it is necessary to fix the linear size of a cell (r_0) and the redshift when the calculations were started (z_{start}). These values are selected on the base of best agreement between the simulation results and (i) observed two-point correlation function (Groth & Peebles 1977) and (ii) data on luminosity function of Abell clusters (Bahcall 1979). It was found that best agreement was reached when $r_0 = 5\,h^{-1}$ Mpc and $z_{start} = 5.25$, where $h = H_0/(100\,\mathrm{km\,s^{-1}\,Mpc^{-1}})$. Unfortunately both numerical and observational data are not very precise and this is the reason why the accuracy of r_0 and z_{start} is not better than 30–50 per cent. Consequently all model parameters have the same uncertainty. The fact that we were able to fit the two functions by using only two parameters (r_0 and z_{start}) gives us more confidence in the model.

With r_0 and z_{start}, fixed this way the rms value of Fourier components of $\delta\rho/\rho$ is 3.2×10^{-5} at the recombination. The spectrum of the density contrast is constrained by ($z = 0$):

$\lambda_{min} = 40\,h^{-1}$ Mpc ($M_{min} = \frac{4}{3}\pi\lambda_{min}^3\bar{\rho} = 1.8 \times 10^{16}\,h^{-1}\,M_\odot$)†

and

$\lambda_{max} = 160\,h^{-1}$ Mpc ($M_{max} = \frac{4}{3}\pi\lambda_{max}^3\bar{\rho} = 1.2 \times 10^{18}\,h^{-1}\,M_\odot$).

The main characteristics of the model are: (1) $\Omega = 1$; (2) the linear size of the cube is $32 \times r_0 = 160\,h^{-1}$ Mpc at $z = 0$; (3) the mass inside the cube is $1.2 \times 10^{18}\,h^{-1}\,M_\odot$; (4) the spectrum of the density perturbations is flat for $\lambda_{min} < \lambda < \lambda_{max}$; (5) on scales $l \lesssim \lambda_{min}/2\pi \simeq 6.4(1+z)^{-1}\,h^{-1}$ Mpc the density contrast weakly depends on l and is approximately equal to 8×10^{-4} at decoupling of the matter and radiation. It seems that this value does not contradict the data on $\Delta T/T$ especially in the neutrino dominated Universe.

3 Method

The investigation of the motion of a large number of particles via self-gravitation was carried out in comoving coordinates. Let $\mathbf{r}$, $\mathbf{u}$, Φ be the coordinated, the velocity and the gravitational potential of a particle, then in the cosmological model the corresponding dimensionless comoving values $\tilde{\mathbf{r}}$, $\tilde{\mathbf{v}}$, $\tilde{\phi}$ are (Shandarin 1980):

$$\tilde{\mathbf{r}} = \frac{1}{a}\frac{\mathbf{r}}{r_0}, \qquad \mathbf{v} = H(t)\mathbf{r} + \tilde{\mathbf{v}}\,\frac{1}{a}\left(\frac{r_0}{t_0}\right), \tag{5}$$

$$t = \frac{2}{3H_0}\left(\frac{\tilde{t}_0}{\tilde{t}}\right)^3, \tag{6}$$

$$\tilde{\rho} = \rho a^3\left(\frac{8\pi G}{3H^2}\right) = \rho a^3/\rho_{crit}(t), \tag{7}$$

$$\Phi = \frac{2}{3}\pi G\rho_{crit}(t)r^2 + \tilde{\phi}\,\frac{1}{a^2}\left(\frac{r_0}{t_0}\right)^2, \tag{8}$$

* Thus the initial amplitude of density perturbations is $\sqrt{\overline{(\delta\rho/\rho)^2}} = \alpha\sqrt{N} \simeq 0.2$ at the scale $\sim 1/k_{max} = (4/\pi)r_0$, where $N = 729$ is the total number of various Fourier harmonics.

† Actually some components with shorter wavelengths are present. The shortest one is $\lambda = \lambda_{min}/\sqrt{3}$, but the number of such harmonics is small. This is so because the amplitudes of Fourier harmonics of $\delta\rho/\rho$ are assumed to be constant (in a statistical sense) inside a cube and not inside a sphere in phase space of $\mathbf{k}$ (3).

with

$$t_0 = \frac{2}{H_0(-\tilde{t}_0)}, \qquad a = \left(\frac{\tilde{t}_0}{\tilde{t}}\right)^2 = \left(\frac{3H_0}{2}\,t\right)^{2/3}, \qquad \tilde{t}_0 < 0, \tilde{t} < 0. \tag{9}$$

Here t_0 is an arbitrary dimensionless constant (connected with z_{start}), r_0 is the constant of linear dimensionality (the cell size). In dimensionless coordinates the equations of motion and the Poisson equations are

$$\frac{d\tilde{\mathbf{v}}}{d\tilde{t}} = -\frac{\partial\tilde{\phi}}{\partial\tilde{\mathbf{r}}}, \qquad \frac{\partial^2\tilde{\phi}}{\partial\tilde{r}_i^2} = \frac{6(\tilde{\rho}-1)}{\tilde{t}^2}. \tag{10}$$

It is worth noting that dimensionless time $\tilde{t}$ is negative. The cosmological singularity corresponds to $\tilde{t} = -\infty$ and $\tilde{t} = 0$ corresponds to infinite future.

The system of equations (10) is solved numerically with the 'cloud-in-cell' method (Hockney 1970). The main steps of this method are the following. (1) We define a space grid (in our case 32 x 32 x 32) and calculate a density at the mesh-points. (2) We compute the gravitational potential at the mesh-points. The discrete analogue of Poisson equation (10) is a system of 32 768 equations that is solved numerically using the fast Fourier transformation. [All the harmonic components are involved when solving the Poisson equation, including the ones whose wavelengths are shorter than $2\pi/k_{\max}$.] (3) The particles are shifted by one time-step in accordance with their velocities and accelerations which were obtained after the numerical differentiation of the potential and the consequent interpolations. The following scheme of integration of the equations of motion was chosen (tildes are omitted):

$$\mathbf{x}^{\text{pr}}_{n+1} = \mathbf{x}_n + \mathbf{v}_n\Delta t + g_n\Delta t^2/2 \equiv \mathbf{x}_n + \mathbf{a}_n + \mathbf{b}_n; \qquad \mathbf{a}_n = \mathbf{v}_n\Delta t, \qquad \mathbf{b}_n = \mathbf{g}_n\Delta t^2/2, \tag{11}$$

$$\mathbf{x}^{\text{corr}}_{n+1} = \mathbf{x}_n + \mathbf{v}_n\Delta t + (2/3\,\mathbf{g}_n + 1/3\,\mathbf{g}^{\text{pr}}_{n+1})\Delta t^2/2 = \mathbf{x}^{\text{pr}}_{n+1} + 1/3(\mathbf{b}_{n+1} - \mathbf{b}_n), \tag{12}$$

$$\mathbf{v}_{n+1} = \mathbf{v}_n + (\mathbf{g}_n + \mathbf{g}^{\text{pr}}_{n+1})\Delta t/2 \Rightarrow \mathbf{a}_{n+1} = \mathbf{a}_n + \mathbf{b}_n + \mathbf{b}_{n+1}. \tag{13}$$

This scheme of integration can be easily modified for the case of variable time-step Δt. The quickly growing value $\tilde{t}^{-2}$ in the Poisson equation is a reason for decreasing Δt.

Our program was checked with the exact one-dimensional solution (Sunyaev & Zeldovich 1972; Doroshkevich, Ryabenki & Shandarin 1973).

$$\tilde{x} = \tilde{q}_x + \frac{1}{\tilde{t}^2}\sin\left[\frac{2\pi}{32}(\tilde{q}_x - 1)\right], \qquad 1 \leqslant q_x < 33 \tag{14}$$

$$\tilde{v}_x = -\frac{2}{\tilde{t}^3}\sin\left[\frac{2\pi}{32}(\tilde{q}_x - 1)\right], \tag{15}$$

$$\tilde{\rho} = \tilde{\bar{\rho}}\left/\left|\frac{d\tilde{x}}{d\tilde{q}_x}\right| = \left\{1 + \frac{1}{\tilde{t}^2}\frac{2\pi}{32}\cos\left[\frac{2\pi}{32}(\tilde{q}_x - 1)\right]\right\}^{-1}, \qquad \tilde{\bar{\rho}} = 1. \right. \tag{16}$$

Solutions (14)–(16) are valid up to the moment of infinite density at the point $\tilde{x} = \tilde{q}_x = 17$, that is up to $\tilde{t}_* = -\sqrt{\pi/16} \approx -0.44$. At the beginning of the test ($\tilde{t}_{\text{start}} = -0.8$) all particles ($32^3$) were homogeneously distributed in $\tilde{y}$ and $\tilde{z}$ directions ($\tilde{q}_y = j, j = 1, 2, \ldots, 32$; $\tilde{q}_z = k$, $k = 1, 2, \ldots, 32$; $\tilde{v}_y = \tilde{v}_z = 0$) but in $\tilde{x}$-direction coordinates and velocity of the particles were fixed in accordance with equations (14) and (15), where $\tilde{q}_x = i, i = 1, 2, \ldots, 32$.

The test was carried out for the special choice of $\Delta\tilde{t}$: $\Delta\tilde{t}_1 = 0.03$ and $\Delta\tilde{t}_n/\Delta\tilde{t}_{n-1} = 0.93$. The test took only 25 time-steps. Some inaccuracies of the method gave rise to the not

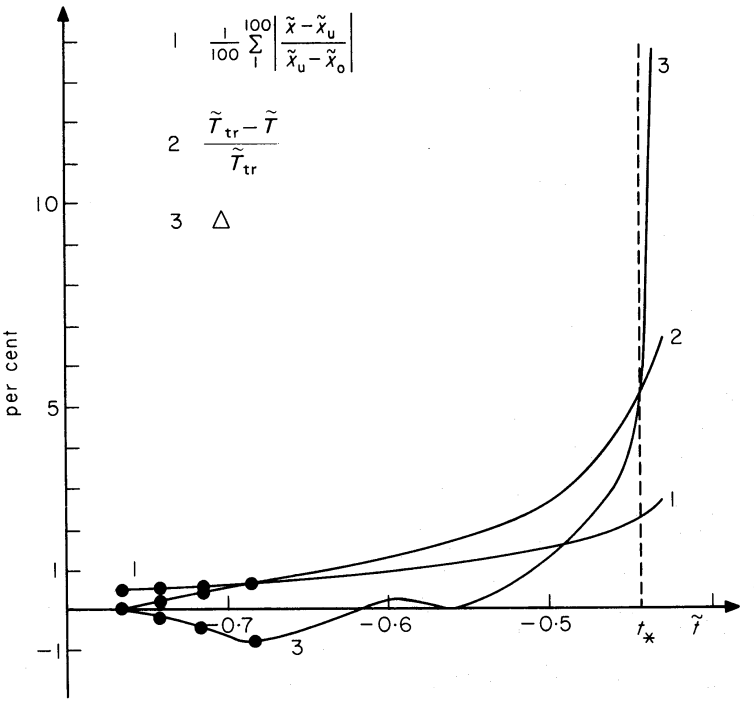

Figure 1. The errors of the one-dimensional test (see equation 19) are plotted as a function of $\tilde{t}$. $\tilde{t}_*$ is the time when a density singularity occurs according to the exact solution. Curve 1 is the rms error of particle coordinates, curve 2 is the deviation of kinetic energy in numerical calculations compared to exact one, and curve 3 is Δ (see equation 19). All values are percentages.

complete accordance with equations (14)–(16) at $\tilde{t} > \tilde{t}_{start}$. The growth of computational errors is illustrated in Fig. 1. The curve 1 gives the errors (percentage) in the displacement of 100 randomly chosen particles. The curve 2 shows the growth of the kinetic energy error of the whole system $\tilde{T}$. $\tilde{T}_{tr}$ is the 'true' kinetic energy:

$$\tilde{T}_{tr} = \frac{1}{2}\int_1^{33} d\tilde{q}_x \tilde{\rho}\tilde{v}_x^2 = \frac{1}{2}\int_1^{33} dq_x \frac{4}{\tilde{t}^6}\sin\left[\pi/16(\tilde{q}_x^{-1})\right] = 32/\tilde{t}^6. \tag{17}$$

During the test $(-0.8 \leqslant \tilde{t} < -0.44)\tilde{T}_{tr}$ increased by a factor of 36 and the difference between $\tilde{T}$ and $\tilde{T}_{tr}$ at the end of computations was only 5 per cent.

The most sensitive accuracy check is based on the Irvine–Dmitriev–Zeldovich theorem, which in variables with tildes, has the form ($\Omega = 1$):

$$\frac{d\tilde{T}}{d\tilde{t}} = \frac{d\tilde{U}}{d\tilde{t}} + 2\tilde{U}/\tilde{t}; \qquad \tilde{T} = \frac{1}{2}\sum_i m v_i^2; \qquad \tilde{U} = \frac{1}{2}\int_V \tilde{\phi}(\tilde{\rho}-1)\,dV = \frac{1}{2}\sum_i \tilde{\phi}_i. \tag{18}$$

Curve 3 in Fig. 1 demonstrates the relative error of the fulfilment of equation (18), that is

$$\Delta = \left[\tilde{T} - \tilde{U} - 2\int_{\tilde{t}_{start}}^{\tilde{t}} \frac{\tilde{U}}{\tilde{t}}\,d\tilde{t} - (\tilde{T}_{start} - \tilde{U}_{start})\right] \Big/ (\tilde{T} - \tilde{U}). \tag{19}$$

The computations of the three-dimensional model, outlined in Section 1, were performed with time-dependent $\Delta\tilde{t}$. At the beginning ($\tilde{t}_{start} = -3$) the time-step was 0.05 and then it decreased with the law $\Delta\tilde{t}_n/\Delta\tilde{t}_{n-1} = 0.98$. At $\tilde{t} = -0.64$, when 142 steps were made, calculations were interrupted. The kinetic energy of the system at the end was 360 times

greater than that at the beginning. The maximum Δ (equation 19) during calculations was $\simeq 14$ per cent, that is it was very close to Δ for one-dimensional test (14)–(16) at $\tilde{t} = \tilde{t}_*$.

4 Evolution of the model

The evolution of the model is demonsrated in Fig. 2. In this figure orthogonal projections of 4000 particles (each eighth) are shown. Fig. 2(a) corresponds to an expansion factor 6.25 from the beginning. It is at this time that the best correspondence to the observed Universe is achieved. This was found from comparison of the observed and simulated both the correlation function and the number densities of rich clusters of galaxies. Large clumps of particles which stand for rich clusters of galaxies can be easily seen in Fig. 2(a). It is possible to recognize some webs connecting these 'clusters of galaxies'. Moreover, wide areas of a

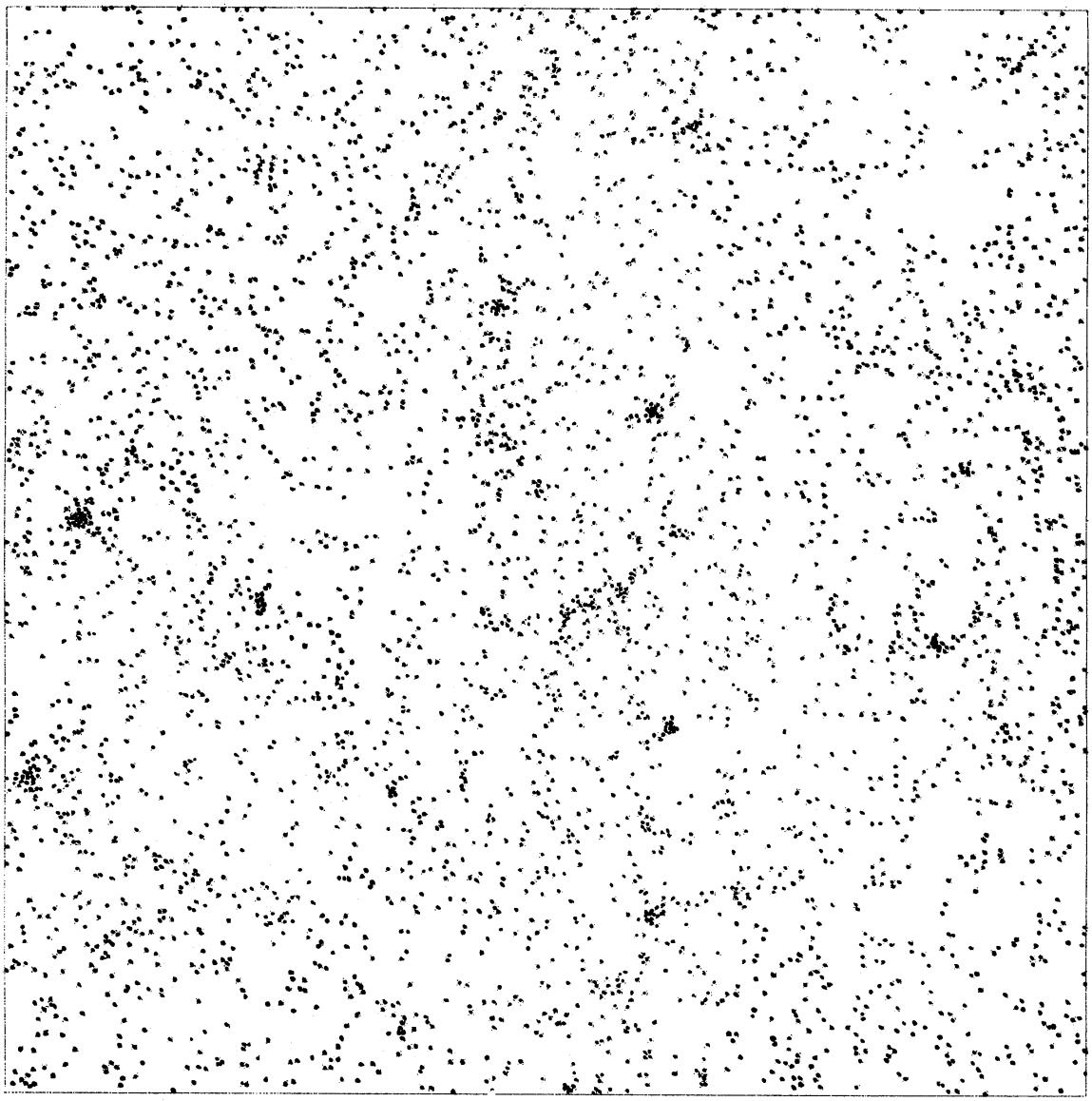

(a)

Figure 2. Three snapshots of the system. (a) Scale factor $a = 6.2\,a_{\mathrm{start}}$ and $(\delta\rho/\rho)_{r_0} = 1.6$; (b) $a = 13.6\,a_{\mathrm{start}}$; $(\delta\rho/\rho)_{r_0} \simeq 3.3$; (c) $a = 18\,a_{\mathrm{start}}$; $(\delta\rho/\rho)_{r_0} \simeq 4.8$. Only each eighth particle is plotted in the figures.

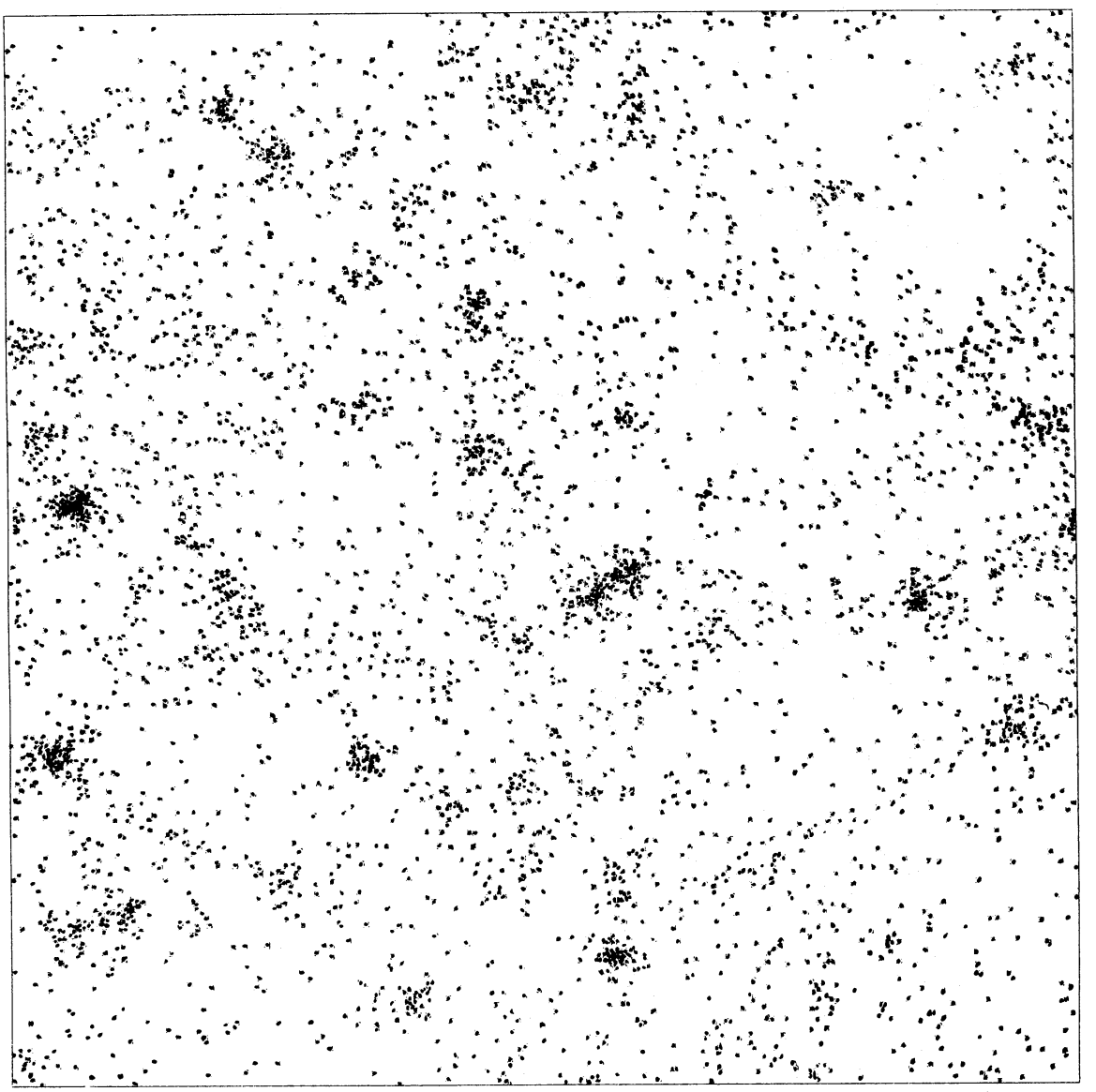

Figure 2 (b)

low density can be found. But except for the clusters, the structure seems to be very washed-out and dim. At this time $(\delta\rho/\rho)_{r_0} = 1.6$. At least part of this effect is explained by reduced number of particles plotted in the figure.

Fig. 2(b) corresponds to the expansion factor 13.6 and $(\delta\rho/\rho)_{r_0} = 3.3$. Beside the clusters one can see very long and massive strings or filaments which tie some clusters together. One also can observe large patches of a very low density. Fig. 2(b) represents the most developed structure.

Later the structure begins to decay and instead of small clusters (at $z = 0$ the whole mass in the clusters is 5–10 per cent), linked by massive bridges–superclusters, the system of isolated big clusters gradually begins to form. The main source of the cluster enhancement is swallowing of superclusters. The stage of evolution is illustrated in Fig. 2(c) [expansion factor is 18 and $(\delta\rho/\rho)_{r_0} = 4.8$].

Fig. 2 shows the distribution of mass density, not that of galaxies. In line with the adiabatic scenario galaxies form only inside regions of high density, that is inside filaments

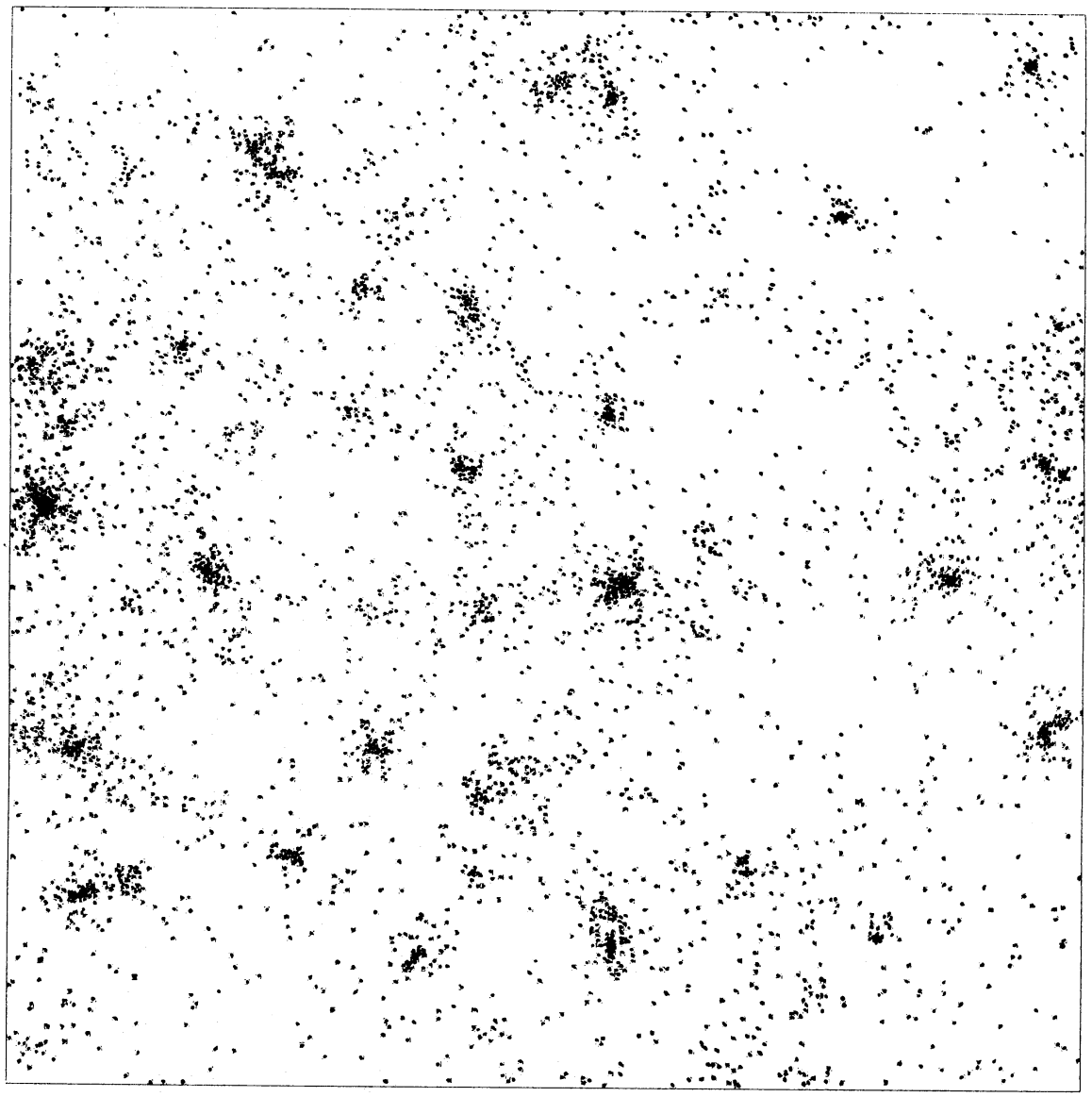

Figure 2 (c)

and perhaps inside pancakes. So galaxy distribution should have a better pronounced structure than that of the matter.

To demonstrate some aspects of the matter density structure, we picked out a sphere of radius $R = 6r_0 = 30h^{-1}$ Mpc with a randomly chosen centre. The sphere contains ~1100 particles and the particles are shown in Fig. 3. To produce an impression of a three-dimensional picture, every particle is drawn as a triangle whose size is inversely proportional to the distance from an observer placed at the distance 1.5 $R = 45h^{-1}$ Mpc from the sphere centre.

In Fig. 3 three different projections of the particle inside the sphere are shown. They were obtained with two successive rotations by 45° around an axis designated by +. One sees that within the sphere there are two rich clusters and two chains. A chain of particles connects the clusters, while another one begins in the bottom cluster, then goes up and left in Fig. 3(c) and leaves the sphere (at the upper left of Fig. 3a) without touching the upper cluster. A very complicated spatial distribution of the particles makes it too difficult to realize the relative location of the chains.

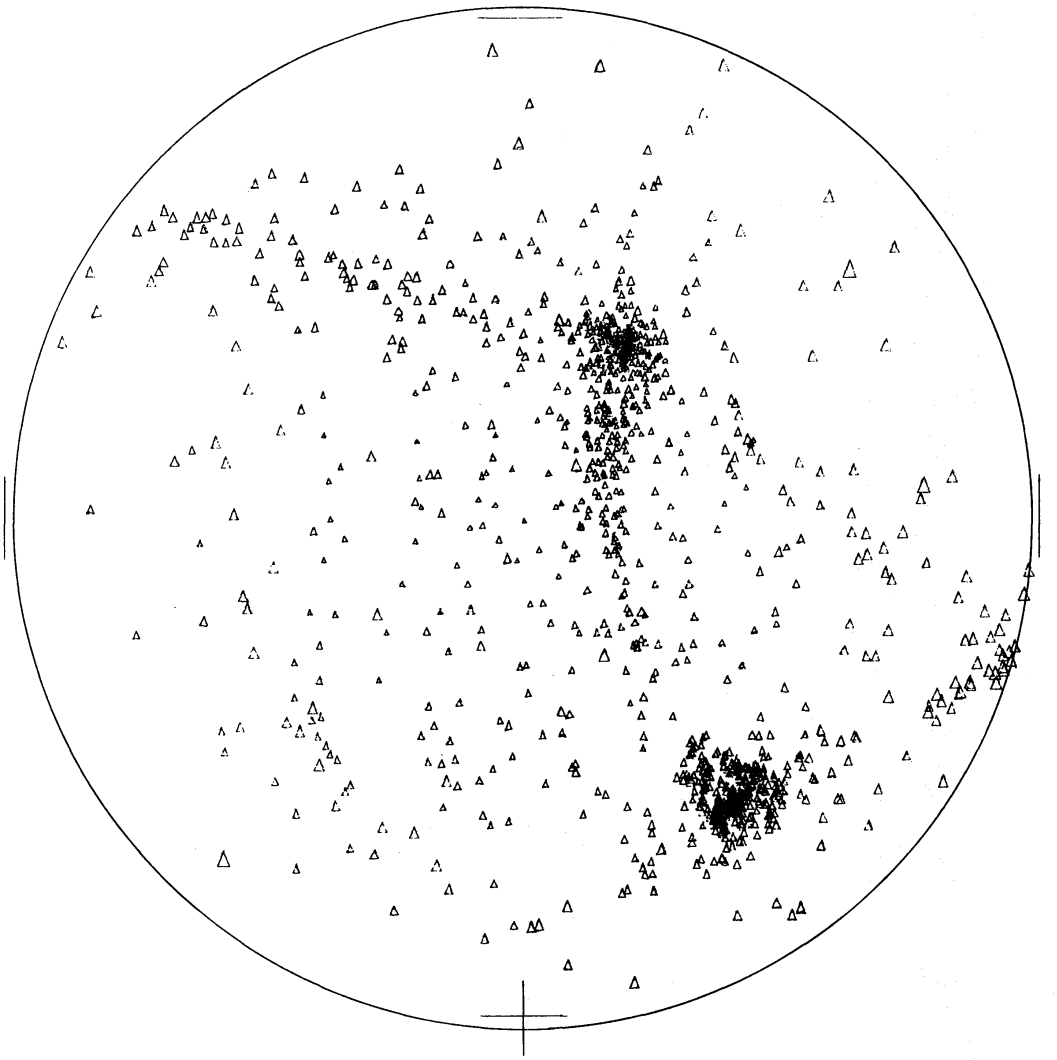

(a)

Figure 3. A small fragment of the particle distribution plotted in Fig. 2(b), when $a = 13.6\,a_{\text{start}}$. As opposed to Fig. 2 here all particles in the sphere with radius $R = 6r_0 = 30h^{-1}$ Mpc are plotted. Every particle is depicted as a triangle whose size is inversely proportional to distance from an observer. The observer is situated at a distance 1.5 R from the centre of the sphere.

A more effective but much more complicated way is to draw a surface of a constant density level. In Fig. 4 a part of a surface defined as $\tilde{\rho} = 2.5\,\tilde{\bar{\rho}}$ ($\tilde{\bar{\rho}}$ is the mean density, $\tilde{\bar{\rho}} = 1$) is shown. It is depicted inside the same sphere. Two dots show the cluster centres. The chains in the figure touch each other near the upper cluster. This is the result of a coarse-grained grid, which was used to define the surface.

The level surfaces constructed over large space reveal that there exists a system of chains (or filaments) extending over the whole volume of the model. The clusters of different richness classes are situated at the points of bifurcation of the chains.

Two-dimensional objects, that is the pancakes, are the most difficult ones to investigate. On the scale 30–50 Mpc the surface of the pancake is far from being a plane, so none of the discussed methods were successful in finding the pancakes. Nevertheless, when placing a plane layer normal to a chain, we observed the particles inside this layer forming strings. Probably these strings result from intersection of the layer with pancakes.

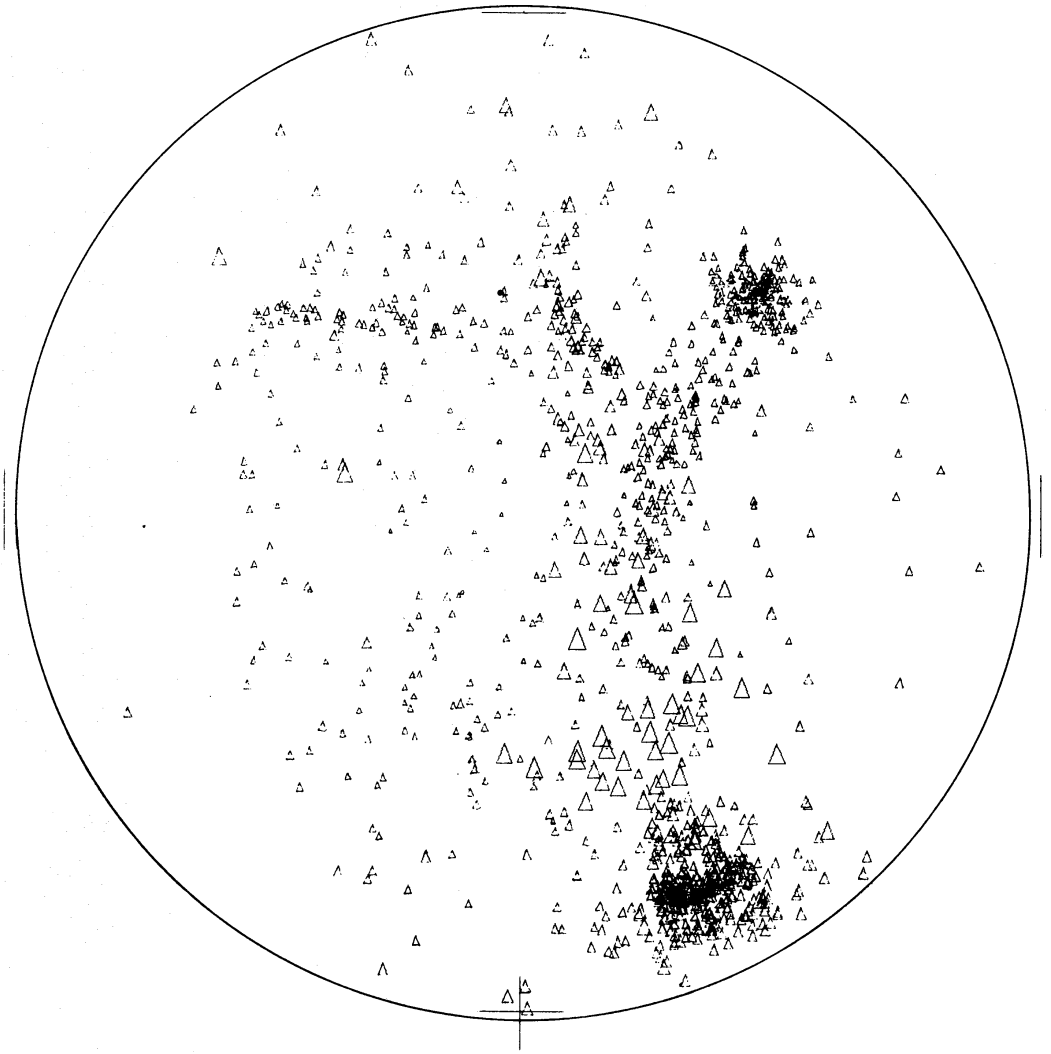

Figure 3 (b)

5 The correlation function

The computation of the spatial two-point correlation function was based on the standard definition:

$$\xi(r) = \frac{N_p}{\bar{r} N_c \Delta V} - 1, \qquad N_c \ll \bar{n} V = N_{tot} \tag{20}$$

where N_p is a number of pairs within the distance interval r, $r + dr$. N_c is a number of randomly chosen centres (in our case $N_c = 450$); $\bar{n}$ is the mean particle density ($\bar{n} = 1$), and $\Delta V = 4\pi/3\,[(r + dr)^3 - r^3]$ is the volume between successive spheres. The usual difficulty arising from sample boundaries is avoided owing to periodicity. At $z = 0$ (which corresponds to Fig. 2a) the resulting $\xi(r)$ is shown in Fig. 5. The correlation function is approximated by a power law $\xi = (3.5\,h^{-1}\,\mathrm{Mpc}/r)^{1.8}$ at $3\,h^{-1} < r < 15\,h^{-1}$ Mpc, being in agreement with observations. At smaller $r (r < 3\,h^{-1}\,\mathrm{Mpc})$ ξ differs significantly from the power-law model. This is the result of the small-scale smoothing inherent in our model. The break of ξ at $r \simeq 15\ h^{-1}$ Mpc ($\xi \simeq 0.1$) probably is not an artefact of our calculations. It indicates the scale separating domains of linear and non-linear regimes. It is worth noting that at the beginning

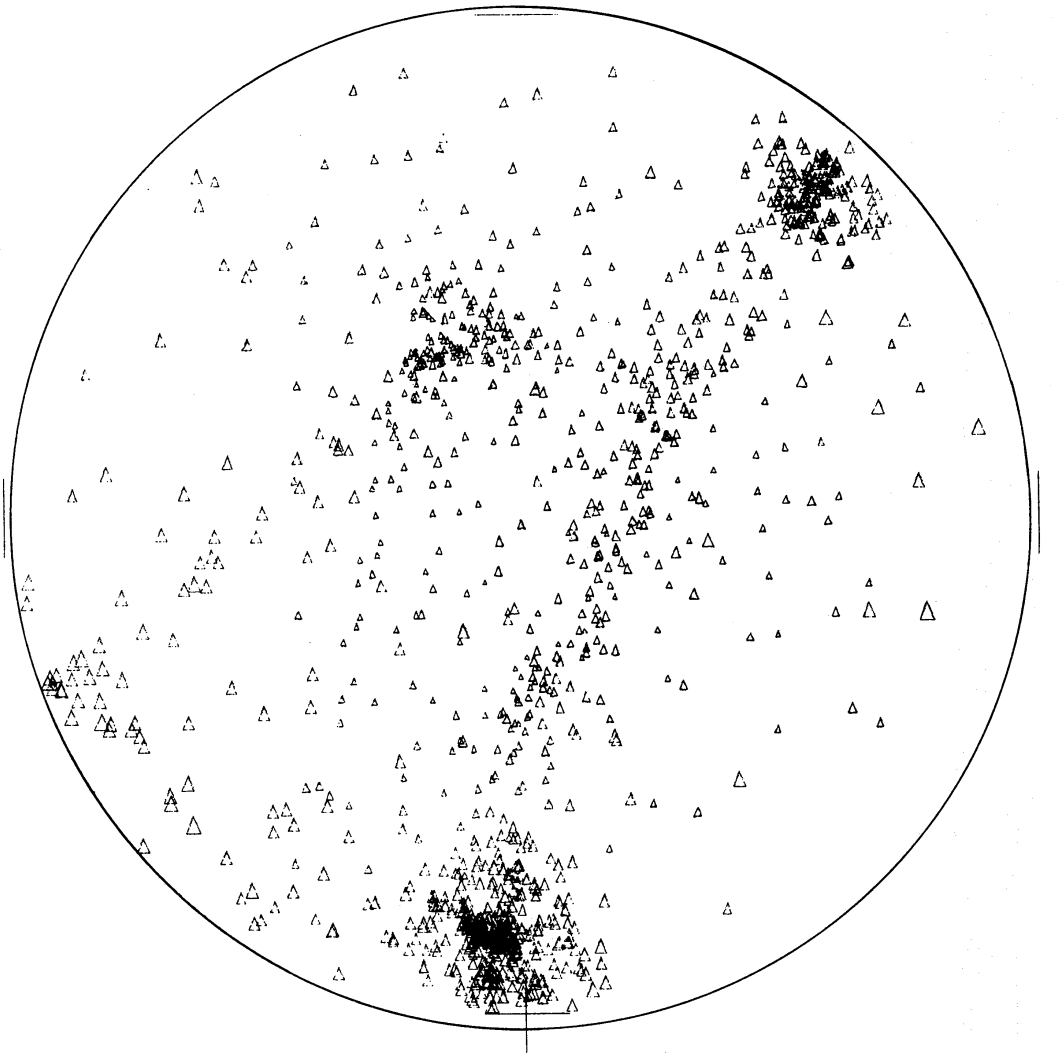

Figure 3 (c)

of the simulations (at the linear state) the correlation function is alternating at $r < 15\ h^{-1}$ Mpc and its amplitude is ~ 0.2. Thus a power-law shape of $\xi(r)$ at $3\,h^{-1} < r < 15\,h^{-1}$ Mpc is entirely determined by non-linear effects. (see for discussion Appendix 1).

The slope of $\xi(r)$ increases with time. It is reasonable to suppose that this is due to transition of the system through several different stages. Every stage is characterized by a fixed kind of object. The first objects inherent in the non-linear stage are pancakes. At this stage $\xi \propto r^{-1}$ on the scales larger than thickness of a pancake ($\sim 5\,h^{-1}$ Mpc) but less than the mean distance between them. Afterwards the stage of filaments, that is one-dimensional objects, comes. At this epoch $\xi \propto r^{-2}$. Of course the real picture is much more complicated because both types of objects exist simultaneously. Besides, the density distribution in the pancakes as well as in the filaments is inhomogeneous. Nevertheless the evolution goes in this way and it gives rise to the increase of the slope of $\xi(r)$.

6 Clusters

As the volume of the model is large enough ($\sim 4 \times 10^6\,h^{-3}$ Mpc^3) there are several tens of rich clusters in it. To compare the number of clusters in the model with the observed one, we used the results of Bahcall (1979) on the luminosity function of Abell clusters. The

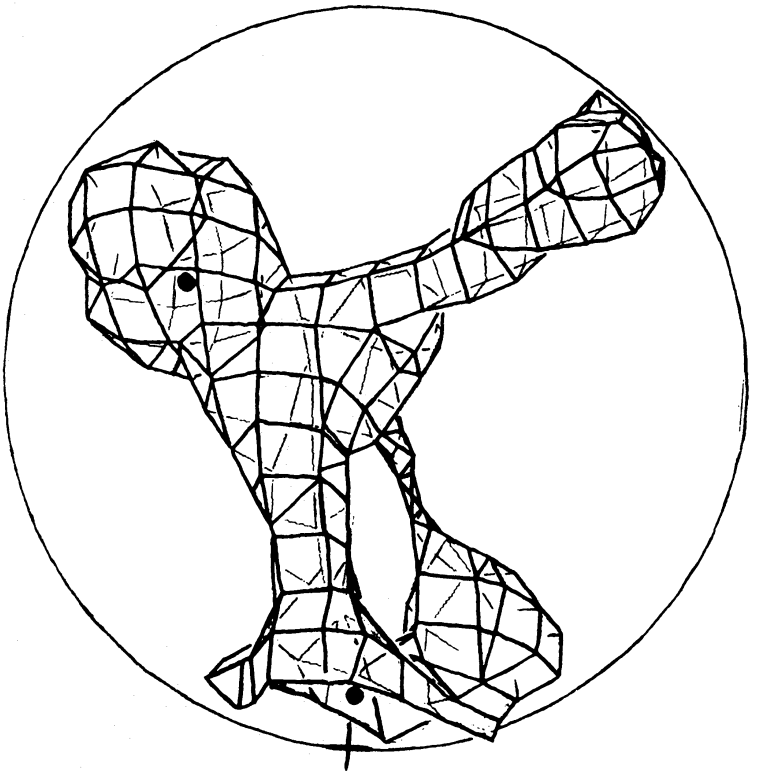

Figure 4. A surface of constant density level is plotted for the same region as that in Fig. 3.

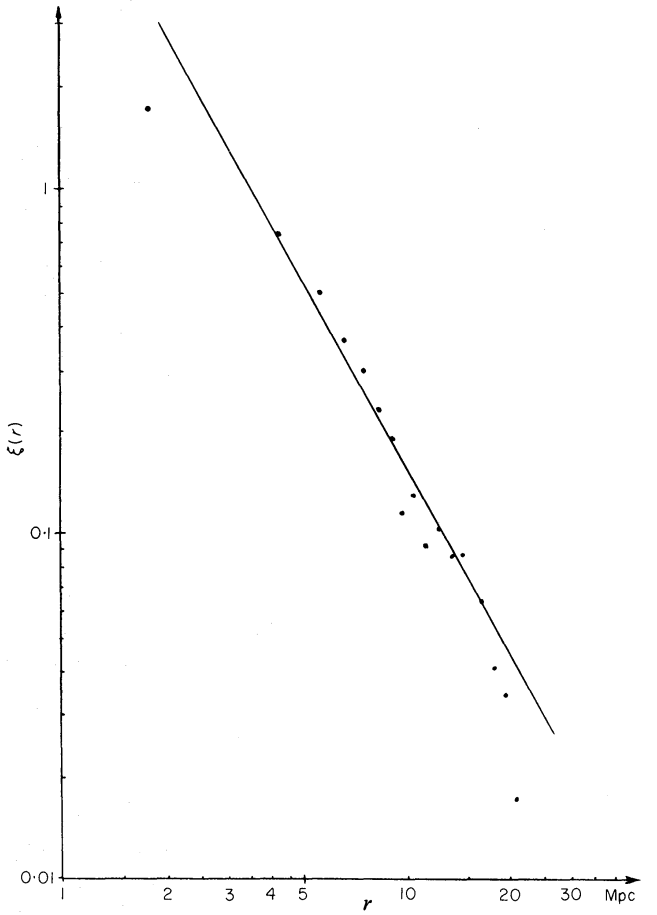

Figure 5. Spatial two-point correlation function computed at the time corresponding to Fig. 2(a). The straight line is a function $\xi = (3.5\,h^{-1}\ \mathrm{Mpc}/r)^{1\cdot 8}$.

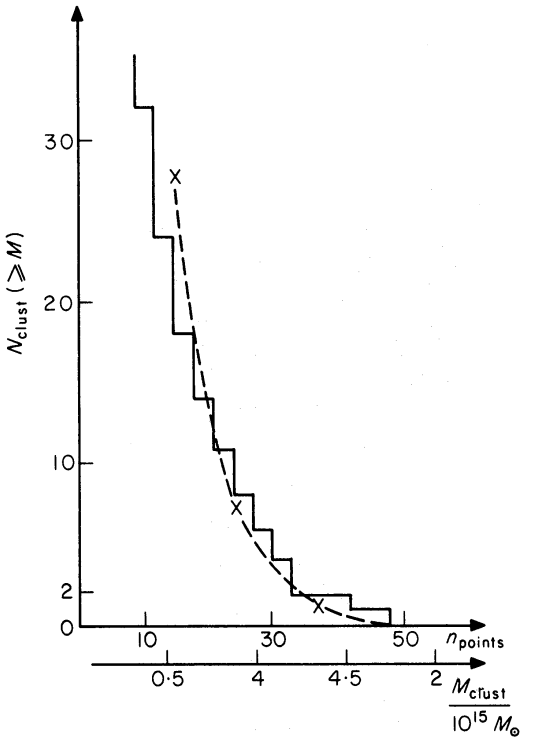

Figure 6. The integral mass function of rich clusters: a histogram represents a model function, crosses are number of Abell clusters in a volume of $(160\,h^{-1}\,\mathrm{Mpc})^3$. When calculating the mass function from the luminosity function the ratio $M/L = 280\,h\,M_\odot/L_\odot$ was used (Bahcall 1979).

magnitude of $M/L = 280\,h\,M_\odot/L_\odot$ was used to obtain the mass distribution of rich clusters. Let us remind the reader that M/L of Coma is estimated to be in the range $240\,h(M_\odot/L_\odot) < M/L < 300\,h(M_\odot/L_\odot)$ (Rood *et al.* 1972; Abell 1977). The radius of a model cluster was chosen to be $1.5\,h^{-1}$ Mpc, that is the same as one used by Abell for the real clusters.

The histogram in Fig. 6 shows the mass function of clusters in the model. Crosses indicate the mean expected in the volume of the model numbers of the Abell clusters of richness greater than richness 1 (upper cross), 2 (middle one) and 3 (lower one).

7 Discussion

The aim of the work is to investigate some aspects of adiabatic scenario in view of the large-scale structure of the Universe.

Our choice of $\Omega = 1$ reflects the present tendency. The constraints on the angular small-scale fluctuations of relict background radiation imply that low fluctuations should be taken at recombination. But this forces us to turn to rather high Ω. Data on neutrino rest mass (Lyubimov *et al.* 1980) if confirmed will justify our choice (see also Doroshkevich *et al.* 1981). However, because of the lack of sufficient observational data, we consider the value $\Omega = 1$ as a possible one.

Our model is in good agreement with the model of the Universe mainly filled with massive neutrinos which interact only through gravity. In this case the evolution of a small part of matter ($\sim 1 \div 10$ per cent) consisting of baryons and electrons – is determined by complicated processes proceeding inside superclusters (i.e. the filaments and pancakes), these processes are similar to those occurring in the models without neutrinos (Sunyaev &

Zeldovich 1972; Doroshkevich, Shandarin & Saar 1978). But the large-scale structure can be well described by a collisionless medium.

Both observational and theoretical arguments give evidence that first objects were formed at $z > 2$. In the model under consideration superclusters contained about 0.1 per cent of the whole mass at $z = 2$. First objects were able to form at this time, but the main part of galaxies probably appeared in the model at $z \simeq 1$. It seems to be somewhat later and we believe that fitting of parameters of the model can push the epoch of galaxies formation to an earlier time.

The main results can be summarized as follows.

(1) In course of non-linear evolution of adiabatic perturbations formation of a system corresponding to the observed two-point correlation function in the range $3h^{-1}$ Mpc $< r <$ $15h^{-1}$ Mpc is possible. Agreement can be gained only during a rather short time interval because the slope of the correlation function increases with time. Scales shorter than $\sim 3h^{-1}$ Mpc were beyond the scope of our simulations.

(2) At that time cluster mass function is close to the observed one.

(3) There is some evidence that side by side with prolate structures oblate ones also exist at the non-linear stage of evolution of adiabatic perturbations. The dimensions and the form of these objects qualitatively correspond to those of superclusters. The prolate systems are much better denoted than the oblate ones.

(4) Both types of structure exist in space in symbiosis.

(5) The regions of high density seem to form a single three-dimensional web structure. However, it is not clear from our simulations whether honeycomb structure arises or not.

(6) The most suitable method for the demonstration of superclusters is drawing a surface of some density level in three-dimensional space. The method should be applied to the real distribution of the galaxies. A possibility of application of the well developed methods for image refinement and processing (Rosenfeld & Weszka 1976) is an advantage of this method.

Acknowledgments

Authors are grateful to Ya. B. Zeldovich and A. G. Doroshkevich for critical and stimulating discussions, one of us (SFS) would also like to thank Dr S. D. M. White for comments on some questions discussed in the article. We also thank Dr G. Efstathiou, who as the referee of our paper has made useful remarks improving both the content and the form of the paper.

References

Aarseth, S. J., Gott, III J. R. & Turner, E. L., 1979. *Astrophys. J.*, **288**, 664.
Abell, G. O., 1977. *Astrophys. J.*, **213**, 327.
Arnold, V. I., 1972. *Functional Analysis and its Application*, **6**, 3.
Arnold, V. I., Zeldovich, Ya. B. & Shandarin, S. F., 1982. *Geophys. Astrophys. Fluid Dynamics*, **20**, 111.
Bahcall, N. A., 1979. *Astrophys. J.*, **232**, 689.
Chincarini, G. & Rood, A. J., 1979. *Astrophys. J.*, **230**, 648.
de Vaucouleurs, G., 1976. *Astrophys. J.*, **203**, 33.
Doroshkevich, A. G., Ryabenki, V. S. & Shandarin, S. F., 1973. *Astrofiz.*, **9**, 257.
Doroshkevich, A. G., Shandarin, S. F. & Saar, E. M., 1978. *Mon. Not. R. astr. Soc.*, **184**, 643.
Doroshkevich, A. G., Kotok, E. V., Novikov, I. D., Polyudov, A. N., Shandarin, S. F. & Sigov, Yu. S., 1980. *Mon. Not. R. astr. Soc.*, **192**, 321.
Doroshkevich, A. G., Kholpov, M. Yu., Sunyaev, R. A., Szalay, A. S. & Zeldovich, Ya. B., 1981. *Proc. Xth Texas Symp. on Relativ. Astrophys.*
Efstathiou, G., 1979. *Mon. Not. R. astr. Soc.*, **187**, 117.
Efstathiou, G. & Eastwood, J. W., 1981. *Mon. Not. R. astr. Soc.*, **194**, 503.

Efstathiou, G. & Jones, B. J. T., 1979. *Mon. Not. R. astr. Soc.*, **186**, 133.
Einasto, J. B., Joeveer, M. & Saar, E. M., 1980. *Mon. Not. R. astr. Soc.*, **193**, 353.
Fall, M., 1978. *Mon. Not. R. astr. Soc.*, **185**, 165.
Gott. III J. R., Turner, E. L. & Aarseth, S. J., 1979. *Astrophys. J.*, **234**, 13.
Gregory, S. A. & Thompson, L. A., 1978. *Astrophys. J.*, **222**, 784.
Groth, E. G. & Peebles, P. J. E., 1977. *Astrophys. J.*, **217**, 385.
Hockney, R. W., 1970. *Methods Comp. Phys.*, **9**, 135.
Kirshner, R. P., Oemler, A., Schechter, P. L. & Shechtman, S. A., 1981. *Astrophys. J.*, **248**, L57.
Lyubimov, V. A., Novikov, E. G., Nozik, V. Z., Tretyakov, E. F. & Kozik, V. S., 1980. *Phys. Lett. B.*, **94**, 266.
Peebles, P. J. E., 1980. *The Large Scale Structure of the Universe*, Princeton University Press.
Rood, H. J., Page, T. L., Kintner, E. C. & King, I. R., 1972. *Astrophys. J.*, **175**, 627.
Rosenfeld, A. & Weszka, J. S., 1976. *Digital Pattern Recognition*, ed. Fu, K. S., Springer-Verlag, Berlin.
Shandarin, S. F., 1980. *Astrofizica*, **16**, 769.
Sunyaev, R. A. & Zeldovich, Ya. B., 1972. *Astr. Astrophys.*, **20**, 189.
Tully, R. B., 1982. *Astrophys. J.*, **257**, 389.
Zeldovich, Ya. B., 1970. *Astr. Astrophys.*, **5**, 84.
Zeldovich, Ya. B., 1978. *The Large Scale Structure of the Universe*, eds Longair, M. S. & Einasto, J., Reidel, Dordrecht, Holland.
Zeldovich, Ya. B. & Shandarin, S. F., 1982. *Pis'ma v A. Zh.*, **8**, 131.

Appendix I

Let us consider in detail some aspects of the evolution and calculation of a two-point correlation function. The correlation function calculated for initial distribution of particles at $z = 5.25$ is shown in Fig. 7 (dash–dotted line). At this time displacement of particles from unperturbed positions in bonds of the regular cubic lattice are small and this influences much the correlation function. Oscillations of the correlation function with distance are explained by similar oscillations of bond numbers in regular lattice compared to that in a statistically homogeneous distribution of particles.

At this time a much better estimation of the correlation function can be done directly from the spectrum of initial perturbations. The well-known relation between spectrum $\langle |\delta_{\mathbf{k}}|^2 \rangle$ and correlation function $\xi(r)$ is given by (Peebles 1980)

$$\xi(r) = \frac{V}{(2\pi)^3} \int d^3k \langle |\delta_{\mathbf{k}}|^2 \rangle \exp(-i\mathbf{kr}) \tag{A1}$$

$$\simeq \frac{V}{(2\pi)^3} \alpha^2 \frac{4\pi}{r^3} (\sin kr - kr \cos kr) \Bigg|_{k_{\min}}^{k^*_{\max}},$$

$$V = (160\, h^{-1}\ \mathrm{Mpc})^3, \qquad \langle |\delta_{\mathbf{k}}|^2 \rangle = \alpha^2 = 6 \times 10^{-5},$$

$$k_{\min} = 2\pi/(160\, h^{-1})\ \mathrm{Mpc}^{-1}, \qquad k^*_{\max} \approx 4\, k_{\min} \sqrt{2}.$$

Here V is the volume of the model; α is a mean amplitude of Fourier components (3); $k_{\min}$ is the wavenumber of the longest wave in the spectrum.

Deriving the second relation we replace the cubic region in the phase space where the initial spectrum was given by the spherical one of equal volume. For flat spectrum it provides equal values of $\xi(0)$ in both cases. This estimate is plotted in Fig. 7 by a dashed line.

At $z = 0$ displacements of particles are large $[(\delta\rho/\rho)_{r_0} \simeq 1.6]$ and initial lattice influences little the correlation function. The solid line in Fig. 7 shows the correlation function at this time. The dotted line shows the power law $\xi(r) = (3.5\, h^{-1}\ \mathrm{Mpc}/r)^{1.77}$.

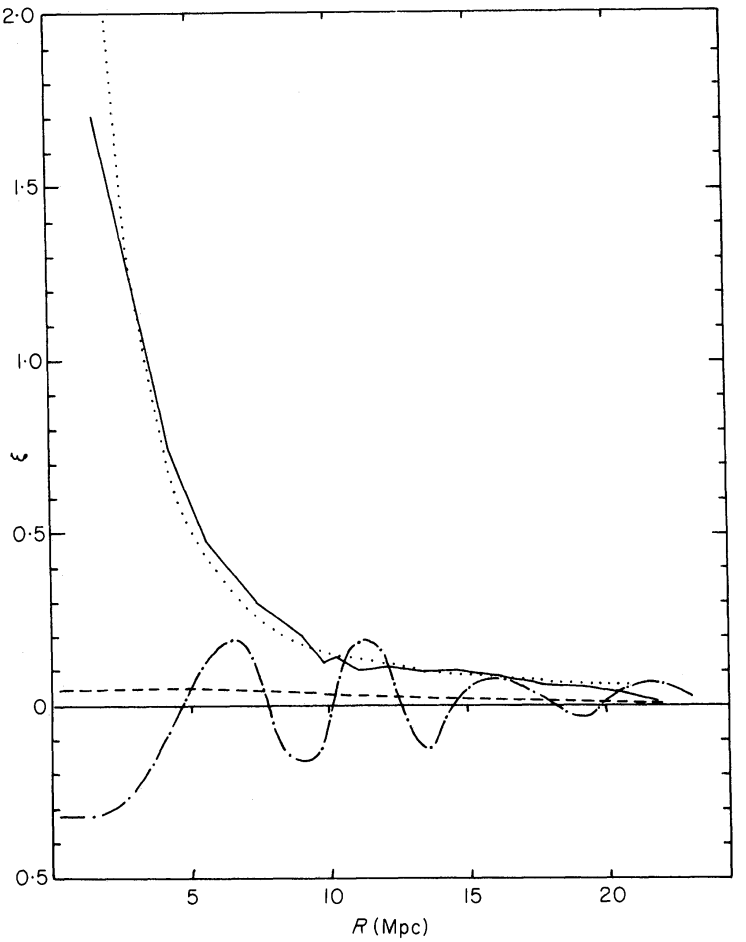

Figure 7. Dash–dot line is the correlation function calculated for the particle distribution at initial time ($z = 5.25$); dashed line is the correlation function estimated by the spectrum at the same time ($z = 5.25$); solid line is the correlation function calculated for the particle distribution at $z = 0$; dotted line is the power law $\xi(z) = (3.5\,h^{-1}\ \mathrm{Mpc}/r)^{1.8}$.

It is interesting to estimate evolution of a quantity

$$D = 4\pi\bar{n}\int_0^R \xi(r) r^2\, dr, \tag{A2}$$

which at linear stage (at $\Omega = 1$) increases as

$$D \propto t^{4/3}. \tag{A3}$$

Numerical integration of $\xi(r)$ at the initial time (A1) over a range from 0 to $20\,h^{-1}$ Mpc of the comoving coordinate gives $D(z = 5.25) \simeq 3.2$. At $z = 0$ the same integral for $\xi(r)$ taken in the form of the power law $\xi = (3.5\,h^{-1}\ \mathrm{Mpc}/r)^{1.77}$ again over the same range (0–$20\,h^{-1}$ Mpc) gives $D(0) = 30$ instead of ~ 120 given by linear law (A3). This shows that the linear extrapolation of (A3) can be dangerous: because of anisotropic collapse the linear law (A3) for $D(20\,h^{-1}\ \mathrm{Mpc})$ is valid within a factor of about 4 despite the fact that $\xi(20\,h^{-1}\ \mathrm{Mpc})$ is much less than unity. Of course this does not put any doubt in the validity of the law (A3) on larger scales. This question will be discussed in detail in a separate paper.